Supporting Information

Rational Design of a Polyphenyl Octacarboxylate HOF for Highly Selective Separation of Benzene Over Cyclohexane

Experimental section

Materials

N, N-Dimethylformamide (DMF), tetrahydrofuran (THF), acetone, benzene (Bz) and cyclohexane (Cy) were obtained from commercial sources and used without further purification.

Synthesis of H_8ETTOB-HOF

The organic octacarboxlyic ligand, H_8ETTOB (4,4',4'',4''',4'''',4''''',4''''''-((ethene-1,1,2,2-tetrayltetrakis(benzene-4,1-diyl))tetrakis(azanetriyl))octabenzoic acid) was prepared according to the literatur.[1] Firstly, 100 mg of H_8ETTOB ligand was dissolved in 30 mL of THF, and then 0.20 mL of the above solution was placed in a 2 mL glass bottle, which was then placed in a 20 mL sealed glass bottle with 2 mL of acetone. Yellow needle-shaped H_8ETTOB-HOF crystals suitable for single crystal X-ray diffraction analysis were obtained by vapor diffusion at room temperature for 48 h. The yield of H_8ETTOB-HOF is 87% (based on H_8ETTOB).

Physical Measurements

Fourier transform infrared spectroscopy (**FT-IR**) was collected on SIR Tracer-100 infrared spectrometer, and the test was conducted using KBr pellet method. The test wavelength ranged from 400 to 4000 cm^{-1}. Thermogravimetric analysis (**TGA**) was performed on a Mettler Toledo TGA2 thermal analyzer from 25 to 800 °C under nitrogen atmosphere at

a heating rate of 10 °C/min. Powder X-ray diffraction (**PXRD**) dates were measured by a Rigaku SmartLab SE diffractometer employing Cu $K_{\alpha,1}$ radiation at 40 kV and 50 mA, scanning over the range 3-35° (2θ) at a rate of 5°/min. H_8ETTOB was prepared according to the literature. Utilizing the Mercury software, simulations were conducted based on the single-crystal data.

Single-Crystal X-ray Crystallography of H_8ETTOB-HOF

The single crystal X-ray diffraction data for the synthesized samples were collected on a Rigaku XtalAB PRO MM007DW diffractometer at 100 K, utilizing graphite-monochromated Cu-Kα radiation (λ = 0.71073 Å). The structure was solved through direct methods and refined by the full-matrix least-squares technique on F2 with the appropriate software incorporated in the SHELXTL program package.[2,3] All non-hydrogen atoms were refined anisotropic displacement. The crystallographic data and relevant information are presented in Table S2 and the CIF files are freely provided by the Cambridge Crystallographic Data Centre (CCDC No. 2375475).

Nitrogen Sorption Measurements

The N_2 adsorption isotherms were measured using an iPore 620 multipurpose gas analyzer, maintaining at 77 K under liquid nitrogen bath. Prior to the measurement, to remove all the guest solvents in the framework, the fresh crystal samples were activated at 473 K with a recirculating control system for 12 h. The specific BET surface area was calculated based on the N_2 adsorption isotherm data. The total pore volume (Vtot) was calculated based on the adsorbed amount of nitrogen at the P/P_0 of 1.0. The PSD was derived from the adsorption branch of N_2 isotherms using the non-local density functional theory method and assuming a slit pore model.

Adsorption selectivity calculation

The dual site Langmuir-Freundlich isotherm model was adopted to fit the adsorption isotherms of Bz and Cy on the H_8ETTOB-HOF, which was described as follows:

$$q = q_{A,sat}\frac{b_A p^m}{1+b_A p} + q_{B,sat}\frac{b_B p^n}{1+b_B p} \quad (1)$$

where q (mol kg^{-1}) represents the adsorption amount under a relative pressure of p (kPa), $q_{A,sat}$ and $q_{B,sat}$ represent the saturated adsorption amount for adsorption sites A and B, respectively, b_A and b_B are constants for species at adsorption sites A and B, respectively.

Variable-Temperature Powder X-ray Diffraction.

For measurements under nitrogen, the temperature of the system was controlled at defined values. Each PXRD was collected 20 min later after the temperature became stable.

Equilibrium Adsorption Measurements

The adsorption isotherms of Bz and Cy were measured using a MircrotracBEL BELSORP-max surface area and porosity analyzer. Prior to the adsorption experiments, HOF-H_8ETTOB sample was thermally activated at 473K for 10 h under dynamic vacuum conditions, especially the vacuum level was less than 10 Pa for no less than 5 h, to ensure complete removal of residual solvents and guest molecules.

Estimation of the Isosteric Heat of Adsorption

Q_{st} is an important indicator to measure the adsorption capacity of an adsorbent, and it is often used to evaluate the strength of the interaction between the adsorbate gas molecules and the adsorbent material at a specific adsorption amount. Generally, the larger the adsorption heat, the stronger the adsorption. At the same time, Q_{st} is also one of the criteria for judging the energy consumption of material regeneration. The isosteric heats of adsorption can be calculated by using the Clausius-Clapeyronequation, which is described as follows:

$$\frac{dP}{P} = \frac{-\Delta H}{R}\frac{dT}{T^2} \quad (2)$$

$$\ln P = -\frac{\Delta H}{RT} + C \quad (3)$$

where P (mmHg) represents the vapor pressure, ΔH (kJ·mol^{-1}) is the isosteric heat of adsorption at specific Bz loading and temperature on the HOF-H_8ETTOB, R is the gas constant with a value of 8.314 J·(mol·K)$^{-1}$, and T (K) represents the measured adsorption temperature. Using this equation, we can select several adsorption isotherms at different temperatures for the same adsorbate, and obtain the adsorption heat of adsorption by comparing the adsorption pressure values corresponding to the same adsorption amount.

Kinetic Adsorption Tests[4]

The kinetic adsorption measurements were performed on a gravimetric sorption analyzer (BSD-VVS), which employs the microbalance technique to accurately monitor transient gas uptake as a function of time. Approximately 90 mg of H_8ETTOB-HOF was loaded into the sample pan and degassed under vacuum at 473 K for 10 h prior to dynamic gas adsorption measurements to ensure complete activation of the porous framework. The kinetic adsorption profiles were obtained by recording the real-time mass change of the sample under isothermal conditions (298 K) at a fixed gas pressure of 200 kPa.

Kinetic Selectivity Calculation[5]

The diffusional time constants (D', D/r^2) were derived using the short-time approximation of the diffusion equation, based on the assumptions of a step change in gas-phase concentration, initially clean beds, and micropore-controlled diffusion.

$$\frac{m_t}{m_\infty} \approx \frac{6}{\sqrt{\pi}} \times \sqrt{\frac{D}{r^2} \times t} - 3\frac{D \times t}{r^2} \qquad \left(\frac{m_t}{m_\infty} < 0.85\right) \quad (4)$$

Where m_t/m_∞ is the fractional adsorption uptake (mmol g^{-1}), D is the intracrystalline diffusivity (m^2 s^{-1}) of the gas molecules in the porous medium, and r is the crystal radius (m). The slope of q_t/q_∞ versus $t^{-1/2}$ is obtained by fitting the plot in the low gas uptake range, and D' was then calculated as the square of the slope multiplied by π/36. In Equation (5), the kinetic selectivity β_{ij} is defined as the ratio of the diffusional time constants:

$$\beta_{ij} = \frac{D}{r_i^2} \Big/ \frac{D}{r_j^2} \tag{5}$$

Dynamic breakthrough experiments

Breakthrough tests were carried out in the auto mixed-gas break through apparatus (BSD-MAB). The mass of H_8ETTOB-HOF that was fed into the column (volume 2 mL) was 0.636 g. The sample was loaded into a glass-packed column and purged with helium gas at 200°C for 2 hours to eliminate residual solvents present on the surface or within the pores. Nitrogen gas was then passed through a stainless-steel bubble generator containing benzene or cyclohexane at a flow rate of 0.6, 0.9 and 1.2 mL·min^{-1}. After repeated observations and confirmations, the mixture ratio of the two vapors was optimized to be an equimolar combination before sample introduction.

The dynamic adsorption capacities of adsorbates, such as benzene and cyclohexane, on HOF-H_8ETTOB are calculated by dynamic breakthrough curves, using the Equation (6).

$$Q = \frac{F \times 10^{-6}}{m} \times \left(C_0 \times t - \int_0^t C_t dt \right) \tag{6}$$

Where Q is the dynamic adsorption capacities, mg g^{-1}; m is the quality of adsorbents, g; C_0 is the initial concentration of adsorbates, mg m^{-3}; C_t is the outlet concentration at t min, mg m^{-3}; F is the total flow of gas, mL min^{-1}.

The separation factor (α) is the ratio of dynamic adsorption amounts of highly adsorbate gas to weakly adsorbate gas, using the Equation (7).

$$\alpha = \frac{q_1/y_1}{q_2/y_2} \tag{7}$$

Where α is the separation factor; q_i is the adsorption amount of adsorbate gas i; y_i is the molar fraction of adsorbate gas i.

Density Functional Theory (DFT) Calculations

The present first-principles calculations were conducted employing the Vienna Ab-initio Simulation Package (VASP).[6] Within this computational framework, the electron-core interactions were treated with high precision using the Projector Augmented Wave (PAW) method,[7] while electron exchange-correlation effects were accounted for through the Perdew-Burke-Ernzerhof (PBE) functional under the generalized gradient approximation (GGA).[8] The implementation utilized a plane-wave basis set with optimized pseudopotentials, ensuring both computational efficiency and accuracy in the electronic structure calculations. The plane-wave cutoff energy was fixed to 500 eV. Given structural models were relaxed until the Hellmann–Feynman forces smaller than -0.02 eV/Å and the change in energy smaller than 10-5 eV was attained. The vacuum thickness was set to be 25 Å to minimize interlayer interactions. During the relaxation, the Brillouin zone was represented by a Γ centered k-point grid of 5×5×1. Grimme's DFT-D3 methodology was used to describe the dispersion interactions among all the atoms in adsorption models. The minimum energy pathway (MEP) for the diffusion reaction, along with the corresponding activation barrier, was calculated using the climbing image nudged elastic band (CI-NEB) method.

Table S1 Physical properties of benzene and cyclohexane.[9]

	Three-dimensional size ($Å^3$)	Polarizability ($cm^3 \times 10^{-24}$)	Kinetic diameter (Å)	B.P. (K)
Benzene	3.3×6.6×7.3	10.0-10.7	5.85	353.3
Cyclohexane	5.0×6.6×7.2	10.8-11.7	6.00	353.9

Table S2 X-Ray crystallographic data for H_8ETTOB-HOF.

Compound	H_8ETTOB-HOF
Empirical formula	$C_{82}H_{56}N_4O_{16}$
Formula weight	1353.30
Temperature (K)	100(2)
Crystal system	Orthorhombic
Space group	*Pbca*
a/Å	43.8500(5)
b/Å	9.0884(2)
c/Å	44.6050(7)
α/°	90
β/°	90
γ/°	90
Volume/$Å^3$	17776.3(5)
Z	8
$\rho_{calc}mg/m^3$	1.011
μ/mm^{-1}	0.583
F(000)	5632
Crystal size/mm	0.23×0.22×0.11
Radiation	Cu
2θrange for data collection/°	3.964 to 76.254
Index ranges	-53<=h<=55, -11<=k<=11, -42<=l<=54
Reflection collected	64822
Independent reflections	17947 (R_{int} = 0.0654)
Data/restraints/parameters	17947/1/927
Goodness-of-fit on F^2	1.062
Final R indexes [I>=2σ (I)]	R_1 = 0.0960, $_wR_2$ = 0.2792
Final R indexes [all data]	R_1 = 0.1487, $_wR_2$ = 0.3149
Largest diff. peak / hole / $eÅ^{-3}$	0.346/-0.239
Completeness	0.963

Table S3 Hydrogen bonds in H_8ETTOB-HOF.

D-H···A	d(D-H)	d(H···A)	d(D···A)	<(DHA)
O(1)-H(1)···O(8)#1	0.84	1.82	2.652(5)	169.9
O(3)-H(3)···O(5)#2	0.84	1.73	2.563(4)	168.2
O(6)-H(6)···O(4)#3	0.84	1.78	2.606(4)	165.6
O(7)-H(7)···O(2)#4	0.84	1.80	2.629(5)	170.0
O(9)-H(9)···O(16)#4	0.84	1.80	2.622(4)	165.3
O(11)-H(11)···O(13)#5	0.84	1.78	2.619(4)	172.5
O(14)-H(14)···O(12)#6	0.84	1.78	2.621(4)	173.1

O(15)-H(15)···O(10)#1	0.84	1.78	2.586(4)	160.1
C(37)-H(37)···O(12)#7	0.95	2.60	3.455(5)	149.8
C(56)-H(56)···O(4)#7	0.95	2.61	3.400(5)	140.9

Table S4 Fitting parameters of dual-site Langmuir-Freundlich (DSLF) model for one-component Bz and Cy adsorption on H_8ETTOB- HOF at different temperatures.

Model		Dual-site Langmuir-Freundlich						
Temper a-ture (K)	Adsor-bates	$q_{A,sat}$ (mmol g^{-1})	b_A (kPa^{-1})	m	$q_{B,sat}$ (mmol g^{-1})	b_B (kPa^{-1})	n	R^2
298		1.698	0.530	1.039	8.918	2417.548	4.253	0.999
318		1.5191	0.002	3.062	1.921	7.504	1.236	0.997
373	Bz	0.899	0.560	0.931	0.974	3.958	0.908	0.999
423		0.371	1.729	1.069	1.119	0.102	1.274	0.998
473		1.136	0.032	1.253	0.333	0.488	1.214	0.999
298		28.602	0.048	0.258	6.254	7570.320	4.494	0.999
318		0.863	4.858	0.725	0.332	0.908	0.550	0.994
373	Cy	0.129	0.042	7.736	0.975	0.634	0.880	0.999
423		0.148	2.545	1.195	1.213	0.099	1.040	0.999
473		0.466	0.250	1.163	1.474	0.098	1.105	0.999

Table S5 The Bz and Cy diffusion coefficients of H_8ETTOB-HOF were measured by BSD-VVS analyzer

Gas	$D/r^2(s^{-1})$

H_8ETTOB-HOF	Bz	0.02057
	Cy	0.00096

Table S6 Kinetic selectivity of H_8ETTOB-HOF was determined using equation (5).

	Kinetic selectivity (Bz/Cy)
H_8ETTOB-HOF	21.4

Table S7 Comparison of HOFs for the adsorptive separation of Bz and Cy

HOF	Bz uptake ($mmol \cdot g^{-1}$)	Cy uptake ($mmol \cdot g^{-1}$)	S_{ads} for Bz/Cy	IAST selectivity	Ref.
HOF-H_8ETTOB[a]	3.92	1.59	2.66	16.5	
HOF-H_8ETTOB[b]	3.14	1.16	2.92	10.2	This work
HOF-H_8ETTOB[c]	1.75	0.98	1.92	19.3	
HOF-Tri-PMDI-Br[a]	4.14	2.09	2.13	-	[10]
AdaOH[d]	1.25	0.04	-	-	[11]
HOF-8[e]	0.89	0	-	-	[12]

Note: [a] [b] [c] represent the adsorption property of HOF at 298 K, 318 K and 373 K, respectively; [d] Utilize nuclear magnetic resonance (NMR) and liquid chromatography in combination for testing; [e]Utilize thermogravimetric analysis (TGA) and NMR for determination.

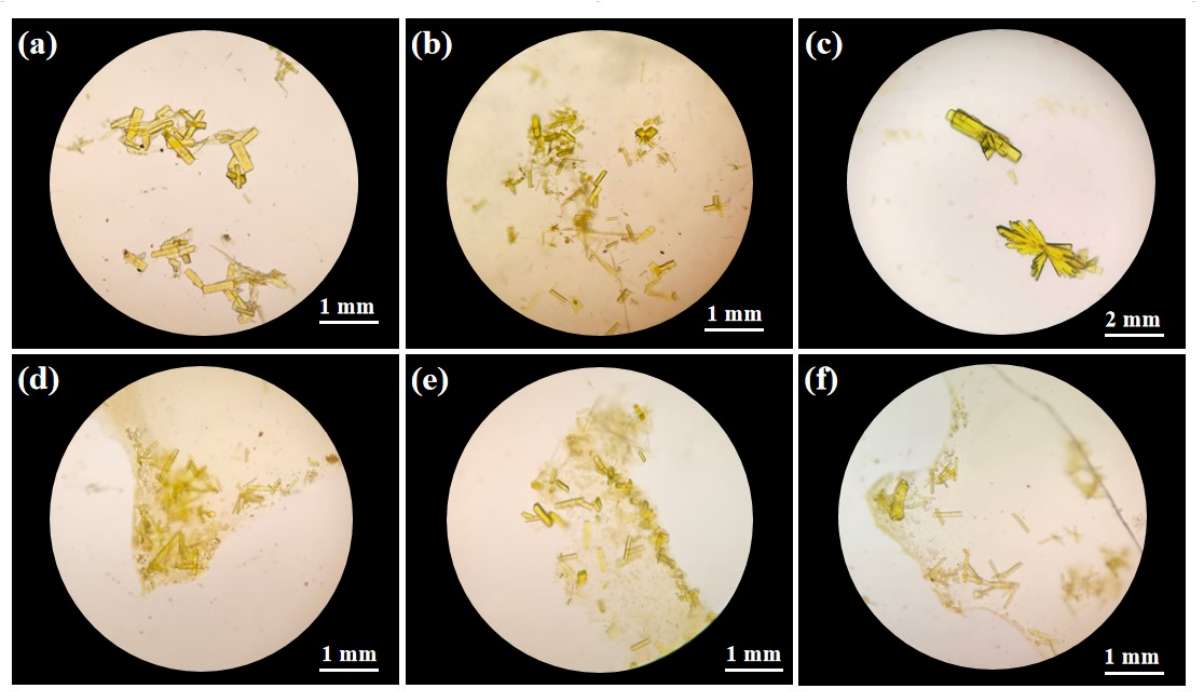

Fig. S1 Optical microscopy images of (a) as-synthesized H_8ETTOB-HOF, (b) soaked in H_2O for three days, (c) soaked in 12 M HCl for three days, (d) soaked in pH=11NaOH for three days, (e) soaked in methanol for three days, (f) soaked in EA for three days.

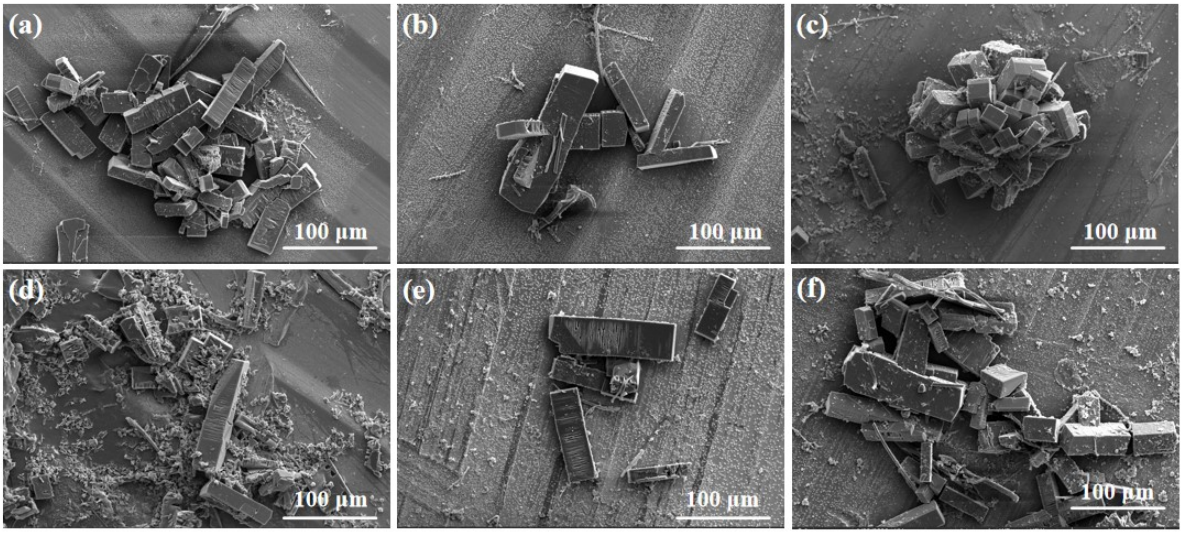

Fig. S2 The scanning electron microscopy (SEM) images of (a) as-synthesized H_8ETTOB-HOF, (b) soaked in H_2O for three days, (c) soaked in 12 M HCl for three days, (d) soaked in pH=11NaOH for three days, (e) soaked in methanol for three days, (f) soaked in EA for three days.

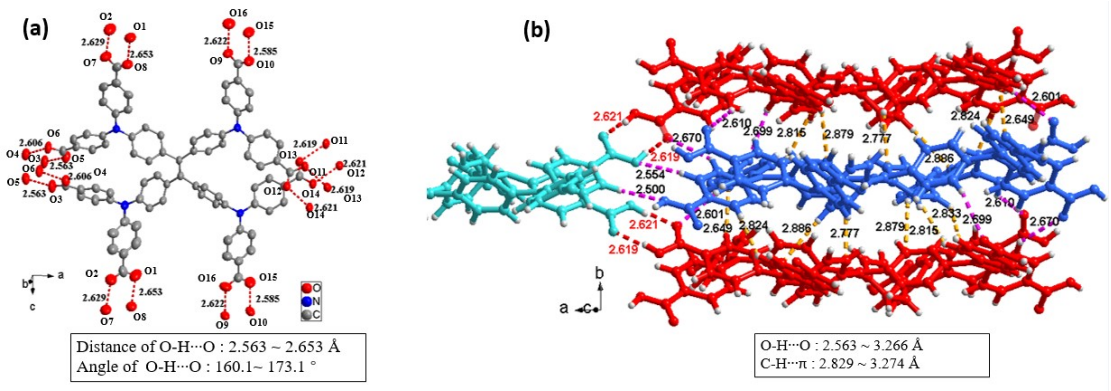

Fig. S3 In H_8ETTOB-HOF, (a) the O-H···O hydrogen-bonds between H_8ETTOB molecules, (b) multiple intermolecular interactions between adjacent layers.

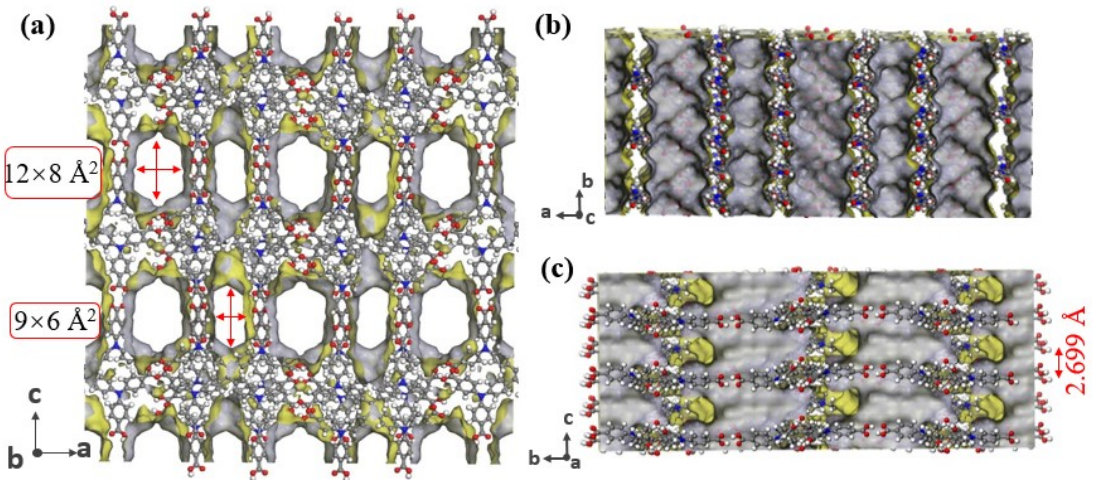

Fig. S4 Images of (a) the microporous structure and the microporous channel structure along the (b) c-axis and (c) a-axis of H_8ETTOB-HOF.

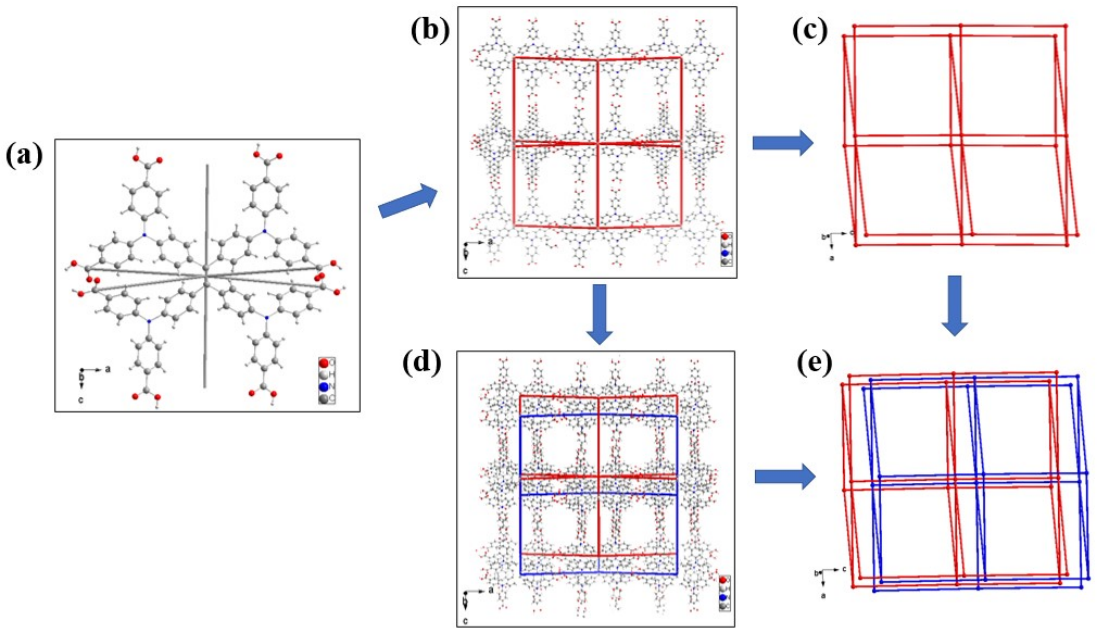

Fig. S5 (a) The molecular structures of H_8ETTOB-HOF unit as 6-connected nodes. The topologies of H_8ETTOB-HOF in (b, c) single-layer and (d, e) two-interpenetrating.

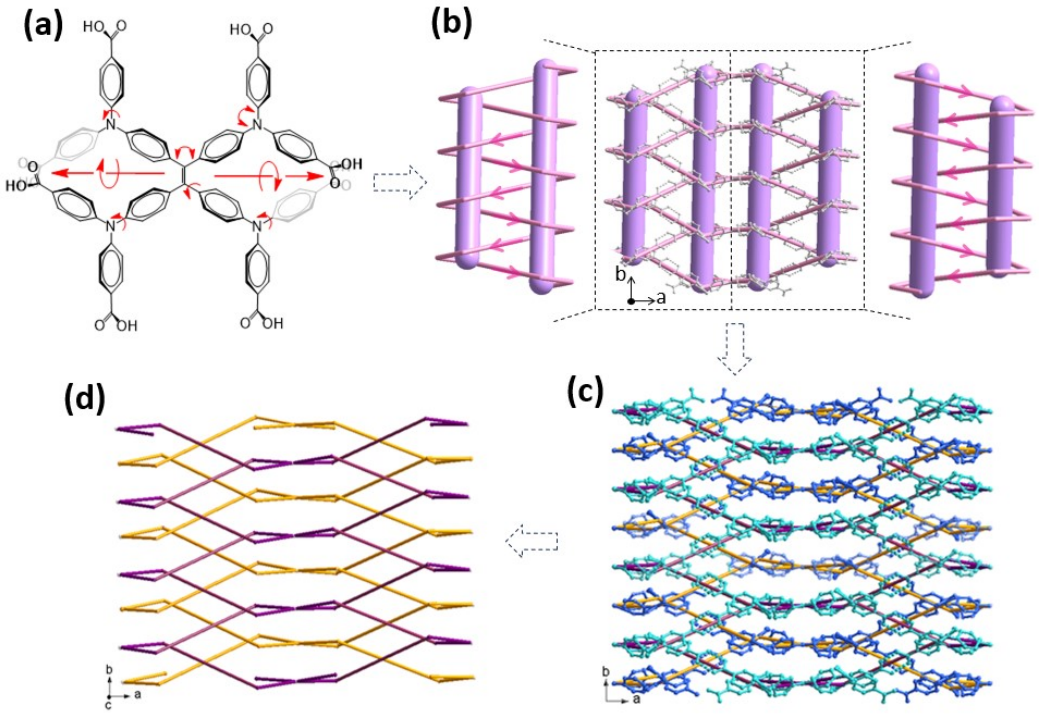

Fig. S6 Crystal Structure of H_8ETTOB-HOF: (a) the chemical structure of the 8-c ligand exhibiting flexible and adaptable structural characteristics facilitated by bond rotation, the presence of a helical axis, and variations in bond angles; (b) single layer displaying a "double-spiral upward figure-eight" pattern along the b-axis; (c) and (d) two-fold interpenetrated H_8ETTOB-HOF displaying a "double-spiral upward figure-eight" pattern along the b-axis.

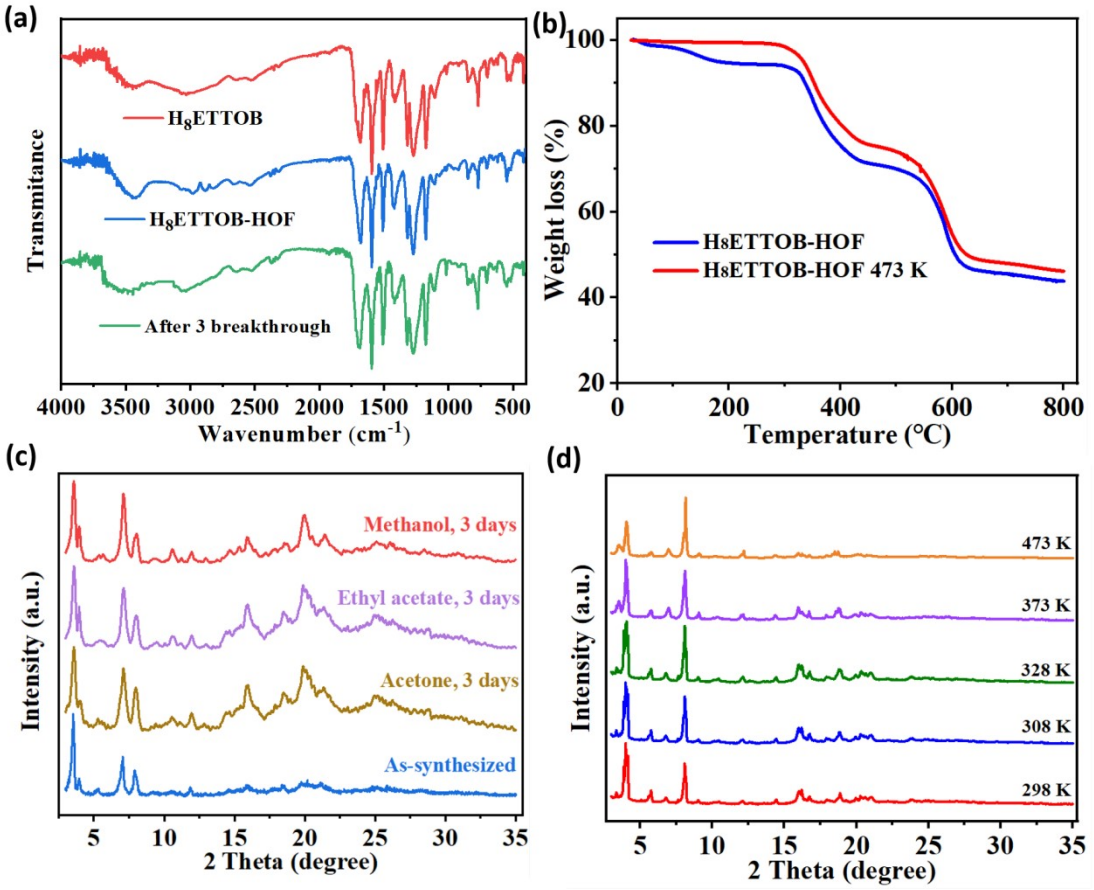

Fig. S7 (a) FT-IR spectra of H8ETTOB-HOF: as-synthesized, activated at 473 K and after three breakthrough cycles. (b) TGA curves of H_8ETTOB-HOF and activated H_8ETTOB-HOF at 473K. (c) PXRD patterns of H_8ETTOB-HOF in some organic solvents. (d) VT-XRD of H_8ETTOB-HOF.

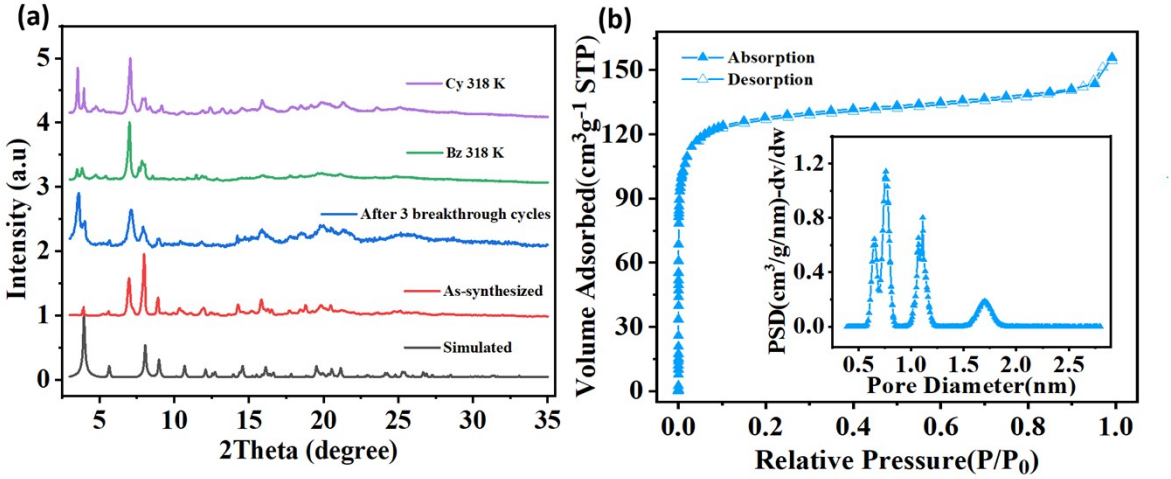

Fig. S8 After 3 breakthrough cycles of (a) PXRD and (b) 77 K N_2 adsorption isotherms.

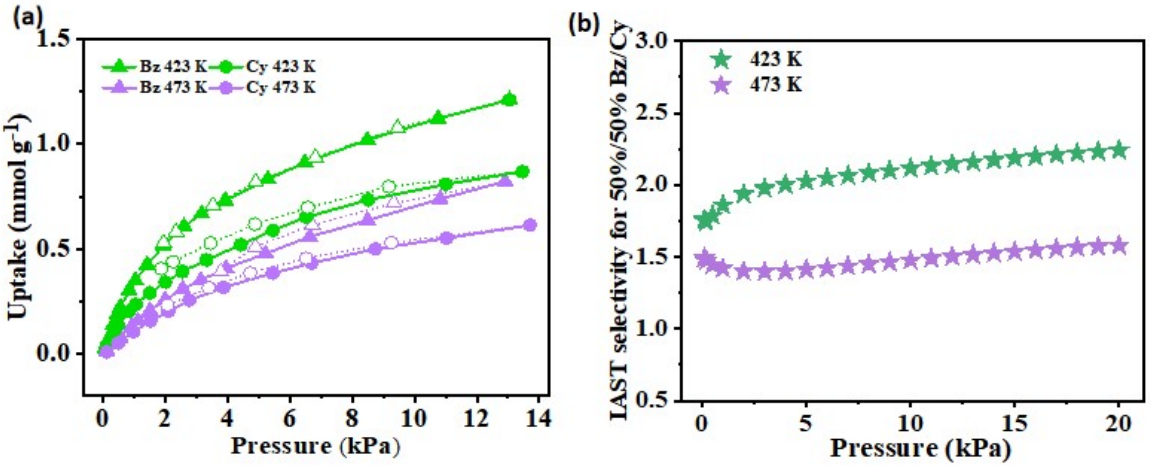

Fig. S9 (a) Single component adsorption/desorption isotherms and (b) IAST selectivity of H_8ETTOB-HOF for storage of Bz and Cy at 423 K and 473 K, respectively. (c) PXRD pattern of regenerated H_8ETTOB-HOF after adsorption of Bz and Cy.

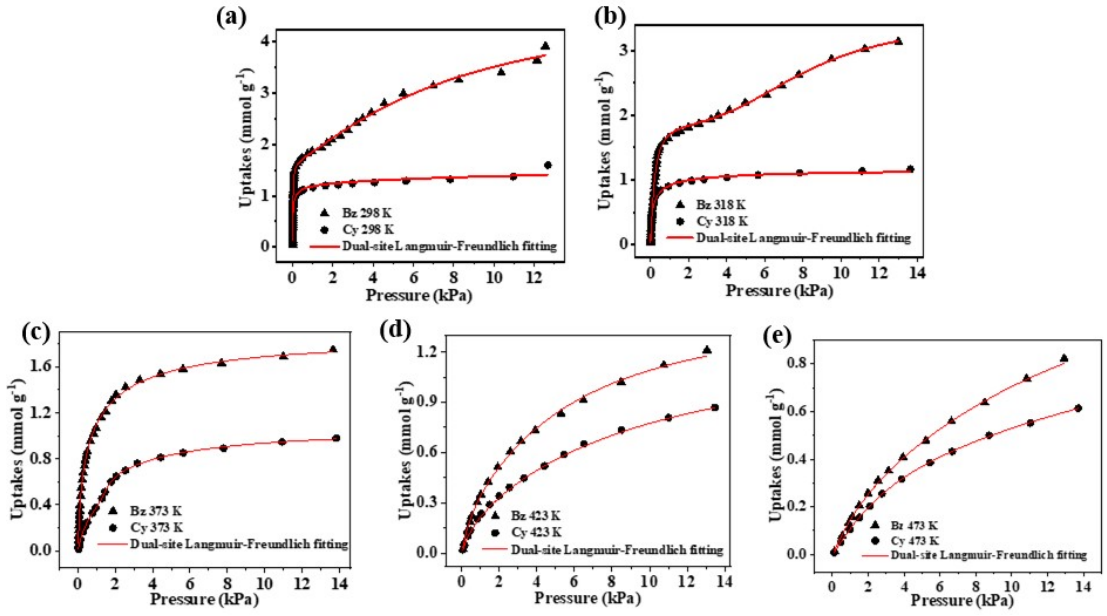

Fig. S10 One-component Bz and Cy sorption data at (a) 298 K, (b) 318 K, (c) 373 K, (d) 423 K and (e) 473 K respectively for H_8ETTOB-HOF and the corresponding non-linear curve fits.

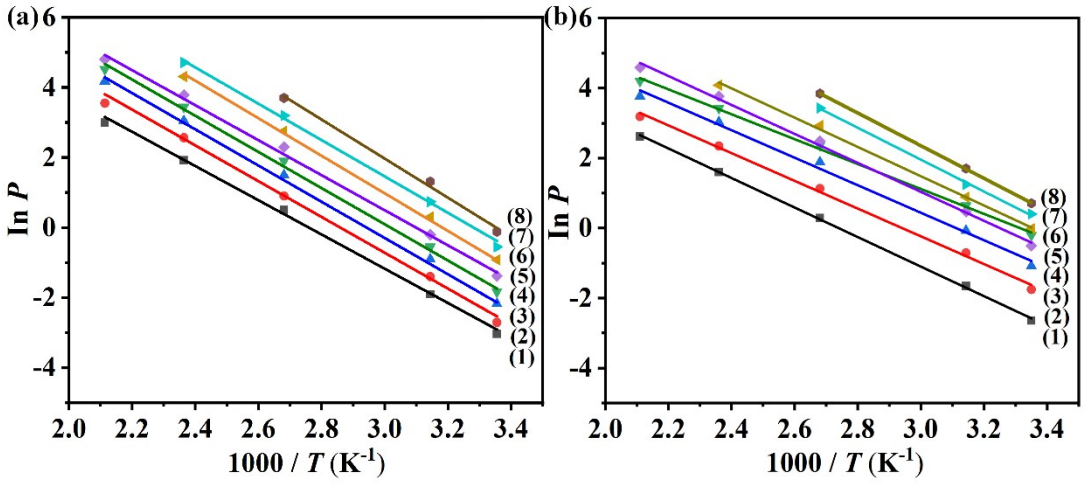

Fig. S11 ln p versus 1/T for the estimation of isosteric adsorption heats of (a) Bz and (b) Cy on the H_8ETTOB-HOF. (a1~8) Q=0.2, 0.4, 0.6, 0.8, 1.0, 1.2, 1.4, 1.6 mmol g^{-1}; (b1~8) Q=0.2, 0.3, 0.4, 0.5, 0.6, 0.7, 0.8, 0.9 mmol g^{-1}.

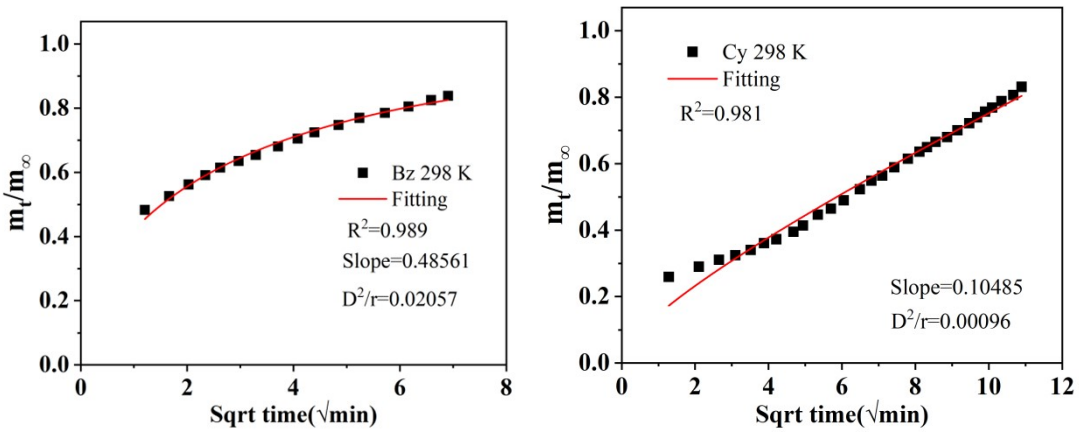

Fig. S12 Diffusional time constant calculation details for H_8ETTOB-HOF towards (a) Bz and (b) Cy.

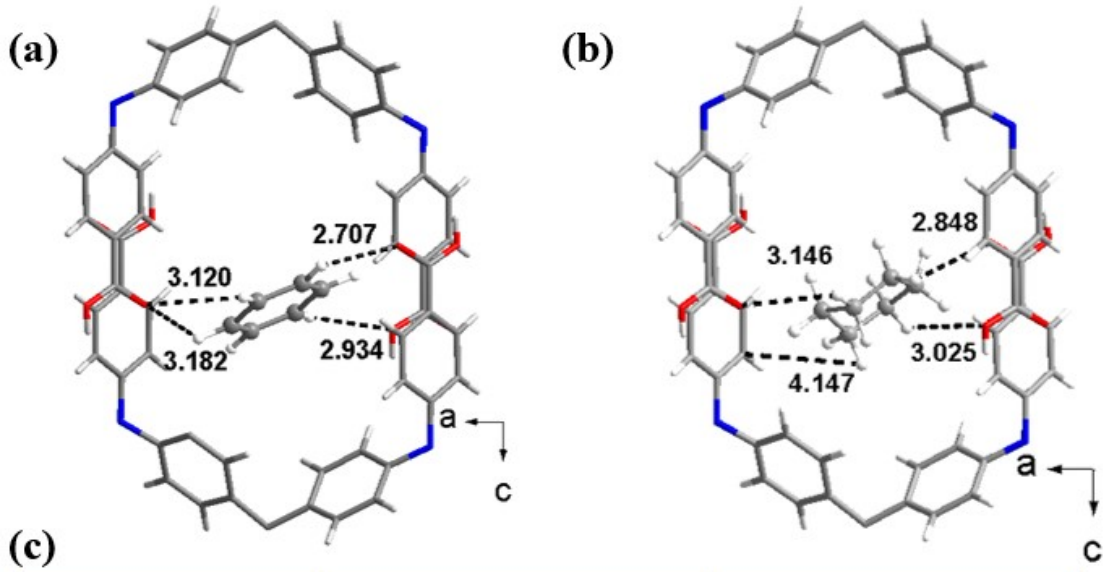

(c)

Host-guest interaction	Bz (Å)	Cy (Å)
C-H···O	2.707	2.848
C-H···O	2.934	3.025
C-H···O	3.120	3.146
C-H···π	3.182	4.147

Fig. S13 (a) Bz and (b) Cy molecules in the H_8ETTOB-HOF (gray: C, white: H, red: O, blue: N). (c) The table of the interaction distance between H_8ETTOB-HOF and Bz and Cy, respectively.

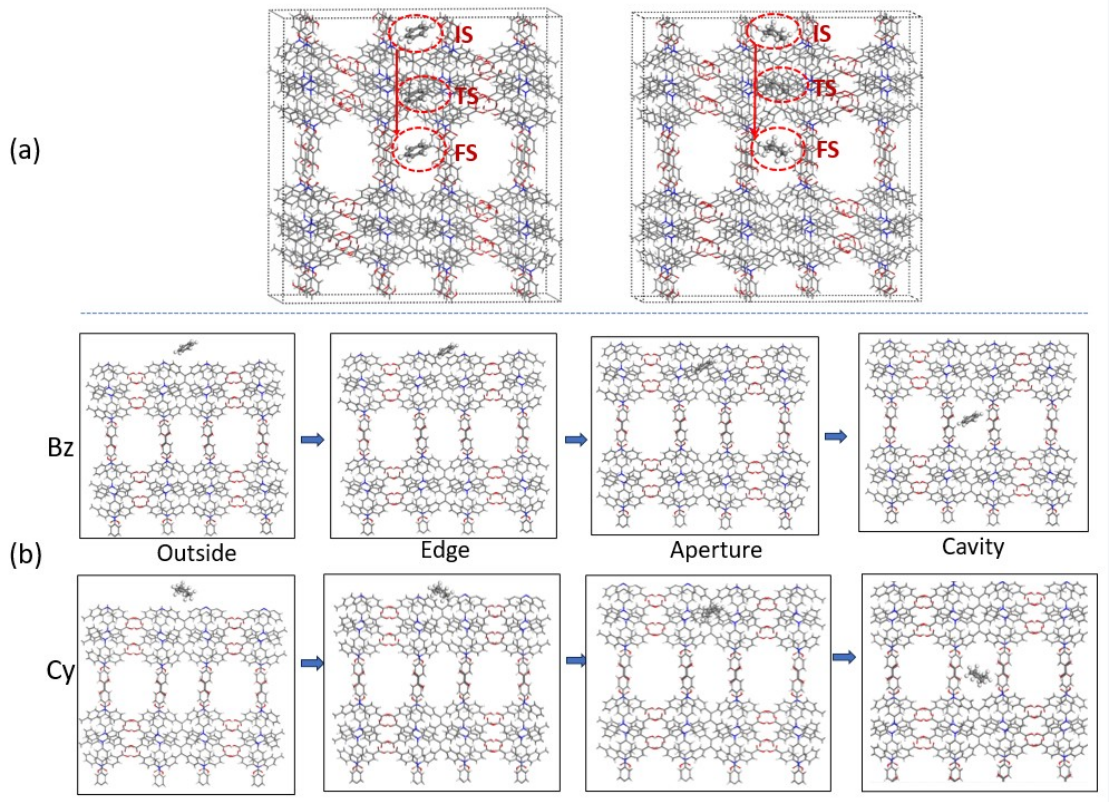

Fig. S14 (a) Spatial distribution of benzene and cyclohexane in H_8ETTOB-HOF under initial state (IS), transition state (TS), and final state (FS) marked. (b) Details of the spatial distribution of benzene and cyclohexane in H_8ETTOB-HOF.

References

1 X. Deng, M. Deng, Y.-L. Li, Z. Liu, T.-F. Liu, X. Chen, S. Cai, B. Liu, J. Li, D. Lv, J. Li and W. Yuan, *Chemical Engineering Journal*, 2023, **474**, 145694.

2 O. V. Dolomanov, L. J. Bourhis, R. J. Gildea, J. A. K. Howard and H. Puschmann, *J Appl Crystallogr*, 2009, **42**, 339–341.

3 G. M. Sheldrick, *Acta Cryst C*, 2015, **71**, 3–8.

4 L. Yang, Y. Liu, F. Zheng, F. Shen, B. Liu, R. Krishna, Z. Zhang, Q. Yang, Q. Ren and Z. Bao, *ACS Nano*, 2024, **18**, 3614–3626.

5 J. Cui, Z. Zhang, L. Yang, J. Hu, A. Jin, Z. Yang, Y. Zhao, B. Meng, Y. Zhou, J. Wang, Y. Su, J. Wang, X. Cui and H. Xing, *Science*, 2024, **383**, 179–183.

6 G. Kresse and J. Furthmüller, *Phys. Rev. B*, 1996, **54**, 11169–11186.

7 G. Kresse and D. Joubert, *Phys. Rev. B*, 1999, **59**, 1758–1775.

8 J. P. Perdew, K. Burke and M. Ernzerhof, *Phys Rev Lett*, 1996, **77**, 3865–3868.

9 C.-H. Liu, L. Chen, H. Zhang, Y. Li, H. Lin, L. Li, J. Wu, C. Liu, Z.-M. Ye, S. Xiang, B. Chen and Z. Zhang, *Chem*, 2023, **9**, 3532–3543.

10 D. Wang and Y. Zhao, *Angewandte Chemie*, 2023, **135**, e202217903.

11 F. Zeng, L.-L. Tang, H. Yu, F.-P. Xu and L. Wang, *Chinese Chemical Letters*, 2023, **34**, 108304.

12 G. Li, J. Chen, B. Song, S. Wang, R. Pan, L. Pei, S. Liu and Q.-Y. Yang, *Separation and Purification Technology*, 2021, **256**, 117781.